Title

Non–ECG-gated myocardial perfusion MRI using continuous magnetization-driven radial sampling

Journal

Magnetic Resonance in Medicine, 72(6)

ISSN

0740-3194

Authors

Sharif, Behzad
Dharmakumar, Rohan
Arsanjani, Reza
et al.

Publication Date

2014-12-01

DOI

10.1002/mrm.25074

Peer reviewed

Published in final edited form as:
Magn Reson Med. 2014 December ; 72(6): 1620–1628. doi:10.1002/mrm.25074.

Non-ECG-Gated Myocardial Perfusion MRI Using Continuous Magnetization-Driven Radial Sampling

Behzad Sharif[1,2], **Rohan Dharmakumar**[1,2,5], **Reza Arsanjani**[1,3], **Louise Thomson**[3,4], **C. Noel Bairey Merz**[2,3,4,5], **Daniel S. Berman**[1,3,5], and **Debiao Li**[1,2,5]

[1]Biomedical Imaging Research Institute, Cedars-Sinai Medical Center, Los Angeles, CA, USA

[2]Department of Biomedical Sciences, Cedars-Sinai Medical Center, Los Angeles, CA, USA

[3]Cedars-Sinai Heart Institute, Cedars-Sinai Medical Center, Los Angeles, CA, USA

[4]Barbra Streisand Women's Heart Center, Cedars-Sinai Medical Center, Los Angeles, CA, USA

[5]David Geffen School of Medicine, University of California Los Angeles, Los Angeles, CA, USA

Abstract

Purpose—Establishing a high-resolution non-ECG-gated first-pass perfusion (FPP) cardiac MRI technique may improve accessibility and diagnostic capability of FPP imaging. We propose a non-ECG-gated FPP imaging technique using continuous magnetization-driven golden-angle radial acquisition. The main purpose of this preliminary study is to evaluate whether, in the simple case of single-slice 2D imaging, adequate myocardial contrast can be obtained for accurate visualization of hypoperfused territories in the setting of myocardial ischemia.

Methods—A T1-weighted pulse sequence with continuous golden-angle radial sampling was developed for non-ECG-gated FPP imaging. A sliding-window scheme with no temporal acceleration was used to reconstruct 8 frames/second. Canines were imaged at 3T with and without coronary stenosis using the proposed scheme and a conventional magnetization-prepared ECG-gated FPP method.

Results—Our studies showed that the proposed non-ECG-gated method is capable of generating high-resolution ($1.7\times1.7\times6$ mm^3) artifact-free FPP images of a single slice at high heart rates (92±21 beats/minute), while matching the performance of conventional FPP imaging in terms of hypoperfused-to-normal myocardial contrast-to-noise ratio (proposed: 5.18±0.70, conventional: 4.88±0.43). Furthermore, the detected perfusion defect areas were consistent with the conventional FPP images.

Conclusion—Non-ECG-gated FPP imaging using optimized continuous golden-angle radial acquisition achieves desirable image quality (i.e., adequate myocardial contrast, high spatial resolution, and minimal artifacts) in the setting of ischemia.

Keywords

myocardial perfusion; first pass; ungated; radial; ischemia; non-ECG-gated

Correspondence: Debiao Li, Ph.D. Biomedical Imaging Research Institute Cedars-Sinai Medical Center 8700 Beverly Blvd., PACT Suite 800 Los Angeles, CA 90048 Tel: (310) 423-7743 Fax: (310) 248-8682 debiao.li@cshs.org.

Introduction

First-pass perfusion (FPP) myocardial MRI is a promising method for accurate diagnosis of coronary artery disease (CAD) (1-4). Despite significant technical advances (5,6), persistent problems have limited the widespread use of myocardial MRI as a modality for routine diagnosis of CAD. One problem is that cardiac MRI (CMR) is generally considered to be a more complex method compared to nuclear myocardial perfusion imaging and more dependent on the expertise of the technologist/operator. Hence, simplification and streamlining of the FPP protocol would increase its accessibility for examining patients with known or suspected CAD.

A major limitation and source of complexity in FPP imaging is the need for near-perfect electrocardiographic (ECG) gating during stress and rest scans. Specifically, the increase in heart rate (HR) variability during vasodilator stress FPP scans can lead to missed slice acquisitions and therefore result in loss of diagnostic information during the short peak-hyperemic time window (6). Such effects are compounded in arrhythmic patients, for whom even rest perfusion imaging can be quite difficult using gated methods. Moreover, reliable ECG gating can be challenging at high fields (e.g., 3T) owing to the amplified magneto-hydrodynamic effects (7). Hence, the need for ECG gating not only increases the overall complexity of the imaging protocol, but also may reduce the clinical utility and diagnostic performance of FPP imaging. Ungated or self-gated CMR methods (8-13) eliminate the need for ECG gating and will help reduce the workflow complexity associated with FPP exams.

FPP imaging without saturation- or inversion-recovery (SR or IR) preparation and instead using “magnetization driven” acquisition was first described by Judd et al. (14) almost two decades ago and has received renewed interest (15,16). Specifically, DiBella et al. (15) proposed using a 3D ungated spoiled gradient recalled echo (GRE) pulse sequence with continuous steady-state acquisition and showed that it can achieve similar contrast properties as SR-prepared GRE in FPP imaging.

In this work, we develop and test a non-ECG-gated FPP imaging scheme using a magnetization-driven RF-spoiled GRE pulse sequence with continuous golden-angle radial sampling of a single 2D slice. The proposed non-ECG-gated FPP imaging method has the following properties: (i) the acquisition is continuous and not synchronized with any gating signal; (ii) the method generates multiple temporally-contiguous FPP images of the same slice per cardiac cycle (rate: 8 frames/s); (iii) image reconstruction is performed without data-sharing between different cardiac cycles – eliminating the possibility of temporal smoothing, which may reduce the temporal fidelity of a FPP image series. Using an animal model with coronary artery stenosis, the presented in-vivo results study the contrast properties and effectiveness of the proposed scheme, dubbed “continuously-sampled” FPP imaging, in comparison to the standard ECG-gated SR-prepared method, referred to as “conventional” FPP imaging.

Methods

Proposed Acquisition Scheme

Conventional FPP pulse sequences are ECG-gated and include a SR magnetization preparation prior to acquisition of each slice (6), in most cases acquired using GRE readouts as shown in Fig. 1(a). Typically, an undersampled Cartesian k-space is acquired (reconstructed using parallel imaging), synchronized with the ECG gating signal at a pre-defined TI time (≈100 ms). The proposed non-ECG-gated magnetization-driven continuously-sampled pulse sequence, depicted in Fig. 1(b), is a continuous fast low angle shot (FLASH) acquisition (RF-spoiled GRE with 50° quadratic RF phase increments) with golden-angle (17) radial k-space trajectory. The T1-weighting and contrast properties of the sequence are magnetization-driven, i.e., the T1 contrast is provided by the approximate steady state magnetization (14). On the reconstruction side, a sliding window (125 ms temporal shifts) is applied to reconstruct 8 frames per second. Radial sampling is used because of its resilience to undersampling (18-21) and cardiac motion (20,22-24). In addition, high-resolution golden-angle acquisition enables retrospective adjustment of spatial/temporal resolution (further described in Image Reconstruction). Thanks to this feature, besides eliminating the need for ECG setup/gating, the proposed method further simplifies the MRI procedure by eliminating the need for choosing/checking the acquisition parameters before the FPP scan.

As has been shown by Di Bella et al. (15), the choice of the flip angle (FA) is crucial for obtaining a desirable myocardial contrast-to-noise (CNR). We used numerical simulations to identify the optimal FA for the proposed pulse sequence. Since the diagnostic task in FPP imaging is to delineate normal and hypoperfused myocardium, our goal in optimizing the FA was to maximize the hypoperfused-to-normal myocardial CNR, hereafter dubbed “perfusion CNR” (pCNR). In contrast to the work in (15), which used the fixed pre-contrast T1 in place of the T1 value for hypoperfused myocardium, our optimization was aimed at maximizing the pCNR for a wide range of normal and hypoperfused myocardial T1s encountered in a FPP scan. The numerical results, which are not included here, indicated that $\alpha = 14°$ is a near optimal FA for achieving the best pCNR for single-slice imaging at 3T with TR = 2.5 ms (similar FA choice as in (15)).

Imaging Experiments

A total of 5 canines were imaged on a 3T clinical scanner (Magnetom Verio, Siemens Healthcare, Erlangen, Germany) with a standard cardiac-torso receiver coil array. Imaging experiments were done under a protocol approved by the Institutional Animal Care and Usage Committee at CSMC. A left thoracotomy was performed and catheters were inserted into the descending aorta and both atria, and were routed through the chest cavity to exit the body. A hydraulic occluder was positioned around the left anterior descending (LAD) artery, and a Doppler flow probe was placed distal to the occluder (both were MR compatible). Animals were allowed to recover for 7 days prior to the imaging studies. On the day of MRI studies, dogs were fasted, sedated, intubated, and anesthetized and placed on the scanner table. Animals were ventilated and positioned on the scanner table in a feet-first right-

anterior oblique position. Continuous physiological monitoring and coronary Doppler flow was performed for the entire the imaging session.

In 4 of the 5 dogs, severe LAD stenosis was inflicted within the MR scanner by inflating the hydraulic occluder, inducing reversible ischemia; the extent of stenosis was confirmed based on Doppler flow velocities. One of the dogs was used as control, i.e., was imaged with no stenosis. Resting FPP data was acquired using the proposed continuously-sampled FPP sequence (Fig. 1(b)) during a ≈30 second breathhold; for comparison, a conventional ECG-gated FPP scan (SR-prepared FLASH) was also acquired. The contrast injection dose (gadoversetamide/ Optimark, Mallinckrodt Inc., Hazelwood, MO, USA) for each perfusion scan was 0.05 mmol/kg with a 14-17 minute time gap in between the two scans to allow for contrast wash out (verified using a TI scout). Each scan was performed 7±2 minutes post stenosis (same level based on Doppler; released after each scan). Delayed enhancement imaging was performed to rule out infarction at the end of the imaging study.

Resting FPP data was acquired using the proposed sequence for continuous non-ECG-gated acquisition of a single short-axis slice at mid ventricle with the following parameters: FA=14° (as described above), acquired in-plane resolution = 1.4 × 1.4 mm^2 with readout FOV = 270 mm and 192 samples per readout, slice thickness = 6 mm, continuous acquisition of 12,500 projections during 31 seconds, TR/TE = 2.5/1.3 ms, rBW ≈ 1370 Hz/pixel. The pulse sequence included gradient-delay correction (prospectively optimized for the scanner (25)), and acquisition of the radial spokes were interleaved based on the golden-angle scheme (17). The parameters for the conventional scan were as follows: SR-prepared FLASH with TI = 100-120 ms, FA = 12°, in-plane resolution = 2.4 × 1.8 mm^2, slice thickness = 6 mm, readout FOV = 295 mm, rBW ≈ 650 Hz per pixel, TR/TE = 2.5/1.3 ms; 2-3 slices per heartbeat; TGRAPPA rate 2. The average HR for the control animal was 57 beats per minute (bpm) and 92±21 bpm for the ischemic animals during the FPP scans (rest imaging).

Image Reconstruction

An important advantage of data acquisition using the golden-angle radial trajectory is the possibility of retrospective selection of reconstruction parameters for balancing the temporal/spatial resolution trade-off. In the context of continuously-sampled FPP imaging as proposed in this work, the parameter to select is the number of projections used for regridding in reconstructing each frame (Fig. 1b) and the trade-off is between streaking artifacts (caused by angular undersampling) and image blurring (caused by cardiac motion). One approach to optimize this trade-off, which we adopt here, is to select the reconstruction parameters based a representative dataset. This approach has been previously used, e.g., in (26) for real-time cine imaging. As shown in Figs. 2(a-c), we used the dataset from one of the ischemic dog studies (HR≈100 bpm) to visually assess the reconstructed image quality corresponding to several choices of the number of projections (limited to Fibonacci numbers (17)). As described in the figure, 89 projections (Panel b) resulted in a sharp image (clear delineation of the subendocardial border) but with a moderate signal-to-noise ratio (SNR ≈ 8.7) due to streaking artifacts; and, 233 projections (Panel c) yielded a relatively high SNR (≈15.1) and no noticeable streaking artifacts – but with significant blurring caused by

cardiac motion. Note that, although 89 projections is 3.4-fold undersampled relative to the Nyquist criterion for 192 readout points (assuming uniform azimuthal sampling), the level of streaking in Fig. 2(b) is relatively low and therefore the in-plane isotropic resolution is determined by the readout pixel size (=1.4 mm); in fact, higher undersampling factors have been used in (18,20) for myocardial imaging. Nevertheless, it is desirable to reconstruct the continuously-sampled frames with a higher SNR than Fig. 2(b) and free of artifacts (streaking/ringing) while avoiding motion-induced blurring seen in 2(c).

It is well known that apodization (windowing of k-space data) improves SNR at the cost of widening the main lobe of the underlying point spread function (PSF) (27-29), resulting in reduced resolution which can be quantified and controlled by measuring the full-width-at-half-maximum (FWHM) of the PSF's main lobe (29,30). Based on this, we used apodization as a simple solution towards the above-mentioned reconstruction goal. Specifically, a Gaussian kernel was employed to weight the projection data (31) along the readout direction and the degree of apodization (width of the Gaussian) was adjusted to result in a 1.2-fold increase in FWHM (compared to non-apodized reconstruction). This implies a reconstruction resolution of 1.7×1.7 mm^2, which—although lower than the acquired resolution—is significantly higher than conventional FPP methods (1.5-times smaller pixel compared to the conventional method). In return for the increase in FWHM, the PSF streaking components (32) are significantly attenuated (resulting in improved SNR); specifically, the 2-norm energy and peak amplitude of streaks are reduced by 1.4-fold and 1.9-fold, respectively. As expected, the apodized reconstruction using 89 projections shown in Fig. 2(d) achieved high SNR ($\approx$14.9) with significantly reduced streaking compared to 2(b). Figure 2(e) verifies the reconstructed resolution based on the FWHM measure. In addition to improving the SNR, this level of apodization effectively eliminates PSF ringing components to preclude ringing-induced dark-rim artifacts (33-36).

Image reconstruction for the continuously-sampled scan was performed offline without any temporal acceleration on a frame-by-frame basis (i.e., each frame reconstructed independent of the others). As described above, each frame was reconstructed using 89 readouts (222 ms temporal window) and the sliding window was then shifted by 50 readouts (125 ms) to reconstruct the next frame, resulting in 8 frames/s. The reconstruction procedure was executed on a workstation (Pentium Dual-CPU Xeon 3.3 GHz) in MATLAB (Mathworks, Natick, MA, USA) using a non-uniform FFT routine (37). With parallel processing (12 cores), the reconstruction time for each frame was about 0.7 s/frame, or a total of 3 minutes per scan. All reconstructed images were converted to DICOM format using tags generated online by the scanner software.

Image Analysis

The first 4 continuously-sampled frames were excluded from the image analysis to allow for transition to steady state (corresponding to 200 RF excitations during the initial 500 ms). Image analysis was performed manually using a DICOM viewer (Osirix by Pixmeo, Bernex, Switzerland). In one of the ischemic dogs (LAD stenosis), the SI-time curves for the continuously-sampled scan were generated by analyzing all diastolic frames (1 frame per cardiac cycle manually selected among 8 frames/s) and measuring the mean intensity inside

3 regions of interest (ROIs): LV bloodpool, normal myocardium, and hypoperfused myocardium. Similarly, SI-time curves were generated for corresponding ROIs in the conventional FPP image series. For each of the ischemic animal studies (n=4), a "representative" frame for the conventional scan was selected from the images acquired during the myocardial enhancement phase that best visualized the perfusion defect. Next, a representative continuously-sampled frame was selected that best matched the corresponding representative conventional FPP frame in terms of (i) myocardial enhancement phase, and (ii) cardiac phase. The former was facilitated by counting the number of heart beats (in the reconstructed continuously-sampled series) from the start of LV enhancement and matching that to the conventional FPP image. Subsequently, for the selected cardiac cycle in the continuously-sampled FPP image series (8 frames/s), one of the frames that best matched the conventional FPP image (in terms of the cardiac phase) was selected.

The myocardium in all representative frames (one conventional and one continuously-sampled for each ischemic study) were manually contoured by two readers to identify a contiguous perfusion defect (hypointense region) in the LAD territory as hypoperfused region, and to select a normal/remote region (similar regions between the continuously-sampled and conventional FPP frames). This was followed by quantitative analysis of: (i) the mean myocardial SI in the ischemic and normal regions for the continuously-sampled images; (ii) measurement of the defect area (in mm^2 units). To compare the contrast properties of the continuously-sampled and conventional FPP images, the difference between mean SI in the normal and hypoperfused regions of the representative frame was computed for all FPP image series. This quantity was then divided by the estimated noise standard deviation (computed as the standard deviation of the SI in the normal myocardial region). The result is the pCNR defined above. The measurements by the two readers were averaged and used for the SI, contrast, and defect area comparisons.

Results

To verify the fast transition to T1-weighted contrast (approximate steady state) for the imaged slice in the continuously-sampled scan, Figs. 3(a)-(b) show the 1^{st} and 5^{th} reconstructed frames for one of the animal studies with coronary stenosis, corresponding to the 0 s and 0.5 s time points during the continuously-sampled scan, respectively. The windowing is kept the same for the two frames and the highlighted box shows a selected ROI adjacent to the heart. Figure 3(c) depicts the mean intensity in the ROI for the first 30 frames (one frame every 125 ms). Comparing (a) and (b) or observing the signal behavior in (c) demonstrates the fast transition to steady state. Specifically, the mean intensity for ROI in 5^{th} frame shown in Panel (b) is only 15% higher than the steady state value (average of the last 10 frames).

In Fig. 4, example FPP images for the conventional and continuously-sampled methods are shown: rows (a)-(b) correspond to the control study (dog with no stenosis) and rows (c)-(d) correspond to one of the ischemic (LAD stenosis) studies. The 1^{st}, 2^{nd}, and 3^{rd} columns show example images from the right ventricular (RV), LV, and myocardial enhancement phases in the FPP image series, respectively. The frames for the continuously-sampled

method were selected so that they closely match the cardiac phase and contrast enhancement phase of the corresponding conventional FPP images. The windowing (gray scale) is kept the same for each row (varies from row to row). The in-plane spatial resolution for the continuously-sampled and conventional FPP images are 1.7×1.7 mm^2 and 2.4×1.8 mm^2, respectively. The average HR for the scans corresponding to rows (c) and (d) were 95 bpm and 98 bpm, respectively. It is seen that the continuously-sampled frames are artifact-free (no streaking or dark-rim) and the myocardial enhancement is clearly seen by comparing the 2^{nd} and 3^{rd} rows. Also, the perfusion defect area in (c3) closely matches the one in (d3).

Figure 5(a) compares the image quality of continuously-sampled and conventional FPP images in terms of CNR (see the figure caption for definition), showing a similar performance (continuously-sampled: 5.82±0.92 vs. conventional: 5.36±0.36; p=0.34). Note that the reported CNR values are not adjusted for the higher resolution/bandwidth and wider acquisition window of the continuously-sampled method compared with the conventional method. We have deliberately avoided such adjustments since it can be argued that the two FPP imaging methods that are being compared (continuously-sampled vs. conventional) differ in several fundamental ways, e.g., in terms of sampling trajectory, reconstruction methods, excitation scheme. These differences are to the extent that it would be more reasonable to compare the image quality (specifically, CNR) of the produced (“end result”) images rather than to retrospectively “adjust” for the differences in acquisition/ reconstruction parameters.

We compared the perfusion defect area (in mm^2 units), measured from the two sets of FPP images (continuously-sampled vs. conventional) across all animals (n=5), and least-squares regression showed a strong agreement (slope = 1.05; intercept = -9.7 mm^2, R^2 = 0.98). A summary of the image contrast analysis for the ischemic dog studies (n=4) are presented in Fig. 5(b,c). The myocardial SI for the continuously-sampled FPP images (average value of the hypoperfused region vs. normal region in the representative frames) are compared in Panel (b). The results show a marked SI difference, which enables delineation of the normal and hypoperfused regions for the continuously-sampled FPP images (normal: 410±69 vs. hypoperfused: 276±42; p<0.005). The result of the hypoperfused-to-normal myocardial CNR (pCNR) comparison between the continuously-sampled and conventional FPP images are described in Panel (c). Overall, the continuously-sampled FPP technique has a similar pCNR compared to the conventional method (continuously-sampled: 5.18±0.70 vs. conventional: 4.88±0.43; p=0.32).

Figure 6 shows the contrast dynamics for the continuously-sampled FPP method in one of the ischemic animals (same dog as Panels (c)-(d) of Fig. 4) and compares the SI-time curves to that of the conventional scan. Panel (a) defines 3 ROIs in: LV bloodpool region, remote myocardial region (normal perfusion), and ischemic region (hypoperfused), respectively. Panel (b) depicts the mean SI in each region (same scale for all plots) for 38 cardiac cycles (2^{nd} to 39^{th} heart beats; average HR: 98 bpm). The two arrows in Panel (b) point to start of LV bloodpool enhancement (arrival of contrast in the LV cavity) and start of myocardial enhancement. Panel (c) shows the SI-time curves for the corresponding conventional scan (average HR: 95 bpm). To better compare the temporal behavior of the myocardial SIs between the continuously-sampled and conventional methods, the myocardial SI-time

curves from the conventional and continuously-sampled scans in (b) and (c) are displayed together in Panel (d) (no normalization or scaling). The dotted line in (d) highlights the myocardial enhancement phase (Panels (c3) and (d3) in Fig. 4), and demonstrates the similar SI difference (contrast) between the normal and hypoperfused curves. Overall, the results demonstrate that the SI-time curves for the continuously-sampled FPP images show a slower contrast uptake (lower upslope) for the ischemic region compared to the remote region, which is consistent with the myocardial SI-time curves for the conventional scan.

Discussion

The need for ECG gating for first-pass perfusion (FPP) myocardial imaging protocols imposes practical difficulties and potentially reduces the diagnostic performance in patients undergoing cardiac exam for the assessment of coronary artery disease (CAD). An accurate, non-ECG-gated FPP technique may help widen the overall adoption of FPP cardiac MRI. In this work, we studied the feasibility and effectiveness of non-ECG-gated FPP imaging using an optimized, high-resolution T1-weighted pulse sequence employing continuous radial sampling with a 2D golden-angle trajectory. Specifically, the presented results demonstrated that, in case of a single-slice 2D imaging, adequate myocardial contrast can be obtained for high-resolution visualization of hypoperfused territories in the setting of myocardial ischemia. The T1-weighting and contrast properties of the sequence are magnetization driven, i.e., are provided by the approximate steady-state magnetization. Our in-vivo results show that the proposed method is capable of generating high-resolution artifact-free FPP images ($1.7\times1.7\times6$ mm^3) of a single 2D slice, while matching the conventional technique in terms of the hypoperfused-to-normal myocardial CNR. Furthermore, the experimental studies in animals show that the perfusion defect areas detected by the continuously-sampled method is consistent with the conventional technique.

To the best of our knowledge, the in-vivo results presented in this work are the first demonstration — in the setting of *myocardial ischemia* — of the effectiveness of a non-ECG-gated FPP method with continuously-sampled magnetization-driven acquisition (i.e., without SR or IR magnetization preparation). It is worth mentioning that the average HRs during FPP imaging for the ischemic animals were quite high (average: 92 bpm) indicating that the proposed method can potentially achieve similar quality for the imaged slice during a vasodilator stress scan wherein such high HRs are typically observed. However, the current method is limited to imaging a single slice during a breathhold using a simple apodized regridding reconstruction with no temporal acceleration or parallel imaging. Extension to accelerated multi-slice or volumetric acquisition (e.g., employing 3D parallel imaging), and invivo studies in patients with varying levels of CAD are needed to further evaluate the clinical effectiveness of the proposed method and its benefits compared to conventional ECG-gated or non-ECG-gated SR-prepared techniques (13,15).

Our results show that the proposed continuously-sampled method yields high-resolution images (1.7×1.7 mm^2 in-plane) and, relative to the conventional FPP method, the perfusion defect can be clearly visualized with good CNR and no dark-rim artifacts (Figs. 4-5). The absence of dark-rim artifacts can be attributed to apodization of k-space data, which effectively eliminates ringing-induced (Gibbs effect) artifacts (33). As demonstrated in Fig.

6, the overall temporal behavior of the signal intensities for the continuously-sampled FPP method is similar to the conventional method. However, comparing Figs. 6(b) and 6(c), the signal saturation effects in the LV bloodpool (nonlinearity between the contrast concentration and image intensity) is significantly higher for the continuously-sampled method compared to the conventional method. In the context of magnetization-driven acquisition, this is due to the low flip angle used, which is optimized for CNR to maximize the sensitivity of the FPP method, but is quite suboptimal in terms of linearity (14,39). Consequently, estimation of an arterial input function and quantitative blood flow assessment can be challenging.

One factor that disturbs the steady-state in continuously-sampled FPP acquisition is T1 changes due to wash in/out of contrast, which generally affects dynamic contrast enhanced MRI. However, we did not observe significant pCNR variation between consecutive diastolic frames during the myocardial enhancement phase, as, for example, seen in Fig. 6(d). This implies that such T1 changes are slow relative to the speed of steady-state transition (from perturbed steady-state back to approximate steady-state). Another process that perturbs the magnetization steady-state is cardiac motion (through-plane motion and in-flow effects during each cardiac cycle), which may result in small but noticeable signal intensity modulations due to changes in T1 sensitivity.

An alternative to GRE-based steady-state acquisition for FPP imaging, as presented in this work or previously by DiBella et al. in (15), is balanced steady-state free precession (SSFP) imaging recently proposed by Giri et al. (16), which maintains steady state by continuously applying the SSFP kernel and uses ECG to synchronize the data acquisition to mid-diastole. In contrast, the presented non-ECG-gated method does not synchronize data acquisition in any way and uses the properties of golden-angle radial acquisition to enable flexible retrospective reconstruction. It is worth mentioning that, based on healthy volunteer studies, the results in (16) indicate that SSFP imaging achieves higher SNR and contrast compared with GRE-based steady-state acquisition.

Study Limitations

We evaluated performance of the continuously-sampled method against a conventional imaging technique. The “gold-standard” for myocardial blood flow comparisons is generally considered to be microsphere-based schemes (40). However, unlike the presented imaging-based comparison, microsphere-based analysis is limited to segmental perfusion assessment and does not allow for a 2D defect contrast and area analysis. Further, the two-reader contouring scheme for measuring the CNR and defect area was used considering the lack of a rigorous threshold-based method for identification of the defect region. As expected, it is not possible to perform such comparisons with perfect accuracy because of the limited resolution and other experiment-related limitations that may cause minor errors.

Conclusions

The presented methods and results demonstrate that non-ECG-gated MRI using magnetization-driven acquisition with optimized continuous radial sampling can achieve desirable image quality (i.e., adequate myocardial CNR, high spatial resolution, and minimal

artifacts) in the setting of myocardial ischemia. The preliminary results presented in this work, which were limited to single-slice 2D imaging, may lay the foundation for future studies on extending the proposed approach to multi-slice 2D or 3D imaging and evaluating its potential benefits in clinical applications.

Acknowledgments

We would like to thank Laura G. Smith, Randy Yang, Avinash Kali, Ivan Cokic, and Richard Tang for help in conducting the imaging experiments.

Grant sponsors: American Heart Association Postdoctoral Fellowship Award 11POST7390063; National Heart, Lung and Blood Institute (NHLBI) grant nos. R01-HL38698, R01-HL091989, R01-HL090957; and, the Barbra Streisand Women's Cardiovascular Research and Education Program, CSMC.

References

1. Miller DD, Holmvang G, Gill JB, Dragotakes D, Kantor HL, Okada RD, Brady TJ. MRI detection of myocardial perfusion changes by gadolinium-DTPA infusion during dipyridamole hyperemia. Magn. Reson. Med. 1989; 10:246–255. [PubMed: 2761383]
2. Rosen BR, Belliveau JW, Vevea JM, Brady TJ. Perfusion imaging with NMR contrast agents. Magn. Reson. Med. 1990; 14:249–265. [PubMed: 2345506]
3. Atkinson DJ, Burstein D, Edelman RR. First-pass cardiac perfusion: evaluation with ultrafast MR imaging. Radiology. 1990; 174:757–762. [PubMed: 2305058]
4. Wilke NM, Jerosch-Herold M, Zenovich A, Stillman AE. Magnetic resonance first-pass myocardial perfusion imaging: clinical validation and future applications. J. Magn. Reson. Imaging. 1999; 10:676–685. [PubMed: 10548775]
5. Gerber BL, Raman SV, Nayak K, Epstein FH, Ferreira P, Axel L, Kraitchman DL. Myocardial first-pass perfusion cardiovascular magnetic resonance: history, theory, and current state of the art. J. Cardiovasc. Magn. Reson. 2008; 10:18. [PubMed: 18442372]
6. Kellman P, Arai AE. Imaging Sequences for First Pass Perfusion - A Review. J. Cardiovasc. Magn. Reson. 2007; 9:525–537. [PubMed: 17365232]
7. Dimick RN, Hedlund LW, Herfkens RJ, Fram EK, Utz J. Optimizing electrocardiograph electrode placement for cardiac-gated magnetic resonance imaging. Invest Radiol. 1987; 22:17–22. [PubMed: 3818232]
8. Debbins JP, Riederer SJ, Rossman PJ, Grimm RC, Felmlee JP, Breen JF, Ehman RL. Cardiac magnetic resonance fluoroscopy. Magn. Reson. Med. 1996; 36:588–595. [PubMed: 8892212]
9. Larson AC, White RD, Laub G, McVeigh ER, Li D, Simonetti OP. Self-gated cardiac cine MRI. Magn. Reson. Med. 2004; 51:93–102. [PubMed: 14705049]
10. Sharif B, Bresler Y. Adaptive Real-time Cardiac MRI Using PARADISE: Validation by the Physiologically Improved NCAT Phantom. IEEE Proc Intl Symp Biomedical Imaging (ISBI). 2007:1020–23. doi: 10.1109/ISBI.2007.357028.
11. Sharif B, Derbyshire JA, Faranesh AZ, Bresler Y. Patient-Adaptive Reconstruction and Acquisition in Dynamic Imaging with Sensitivity Encoding (PARADISE). Magn. Reson. Med. 2010; 64(2):501–513. [PubMed: 20665794]
12. Uecker M, Zhang S, Frahm J. Nonlinear inverse reconstruction for real-time MRI of the human heart using undersampled radial FLASH. Magn. Reson. Med. 2010; 63:1456–1462. [PubMed: 20512847]
13. Harrison A, Adluru G, Damal K, Shaaban A, Wilson B, Kim D, McGann CJ, Marrouche NF, DiBella EVR. Rapid ungated myocardial perfusion cardiovascular magnetic resonance: preliminary diagnostic accuracy. J Cardiovasc Magn Reson. 2013; 15(1):26. [PubMed: 23537093]
14. Judd RM, Reeder SB, Atalar E, McVeigh ER, Zerhouni EA. A magnetization-driven gradient echo pulse sequence for the study of myocardial perfusion. Magn. Reson. Med. 1995; 34:276–282. [PubMed: 7476088]

15. DiBella EVR, Chen L, Schabel MC, Adluru G, McGann CJ. Myocardial perfusion acquisition without magnetization preparation or gating. Magn. Reson. Med. 2011; 67:609–613. [PubMed: 22190332]
16. Giri S, Xue H, Maiseyeu A, Kroeker R, Rajagopalan S, White RD, Zuehlsdorff S, Raman SV, Simonetti OP. Steady-state first-pass perfusion (SSFPP): A new approach to 3D first-pass myocardial perfusion imaging. To appear in Magn. Reson. Med. 2013 doi: 10.1002/mrm.24638.
17. Winkelmann S, Schaeffter T, Koehler T, Eggers H, Doessel O. An optimal radial profile order based on the Golden Ratio for time-resolved MRI. IEEE Trans. Med. Imaging. 2007; 26:68–76. [PubMed: 17243585]
18. Peters DC, Epstein FH, McVeigh ER. Myocardial wall tagging with undersampled projection reconstruction. Magn. Reson. Med. 2001; 45:562–567. [PubMed: 11283982]
19. Peters DC, Ennis DB, McVeigh ER. High-resolution MRI of cardiac function with projection reconstruction and steady-state free precession. Magn. Reson. Med. 2002; 48:82–88. [PubMed: 12111934]
20. Shankaranarayanan A, Simonetti OP, Laub G, Lewin JS, Duerk JL. Segmented k-Space and Real-time Cardiac Cine MR Imaging with Radial Trajectories. Radiology. 2001; 221:827–836. [PubMed: 11719686]
21. Larson AC, Simonetti OP, Li D. Coronary MRA with 3D undersampled projection reconstruction TrueFISP. Magn. Reson. Med. 2002; 48:594–601. [PubMed: 12353275]
22. Glover GH, Pauly JM. Projection Reconstruction Techniques for Reduction of Motion Effects in MRI. Magn. Reson. Med. 1992; 28:275–289. [PubMed: 1461126]
23. Rasche V, Boer RWD, Holz D, Proksa R. Continuous radial data acquisition for dynamic MRI. Magn. Reson. Med. 1995; 34:754–761. [PubMed: 8544697]
24. Tsao J, Boesiger P, Pruessmann KP. Lattice permutation for reducing motion artifacts in radial and spiral dynamic imaging. Magn. Reson. Med. 2006; 55:116–125. [PubMed: 16323156]
25. Peters DC, Derbyshire JA, McVeigh ER. Centering the projection reconstruction trajectory: Reducing gradient delay errors. Magn. Reson. Med. 2003; 50:1–6. [PubMed: 12815671]
26. Kolbitsch C, Prieto C, Schaeffter T. Cardiac functional assessment without electrocardiogram using physiological self-navigation. To appear in Magn. Reson. Med. 2013 doi: 10.1002/mrm.24735.
27. Harris FJ. On the Use of Windows for Harmonic Analysis with the Discrete Fourier Transform. Proceedings of the IEEE. 1978; 66(1):51–83.
28. Pipe JG. Reconstructing MR images from undersampled data: Data-weighting considerations. Magn. Reson. Med. 2000; 43:867–875. [PubMed: 10861882]
29. Liang, Z-P.; Lauterbur, PC. Principles of magnetic resonance imaging. Wiley-IEEE Press; 2000.
30. Epstein, CL. Introduction to the mathematics of medical imaging. SIAM Press; 2008.
31. Naylor DA, Tahic MK. Apodizing functions for Fourier transform spectroscopy. J Opt Soc Am A. 2007; 24:3644–3648.
32. Scheffler K, Hennig J. Reduced circular field-of-view imaging. Magn. Reson. Med. 1998; 40:474–480. [PubMed: 9727952]
33. Sharif B, Dharmakumar R, LaBounty T, Arsanjani R, Shufelt C, Thomson L, Bairey Merz CN, Berman DS, Li D. Towards elimination of the dark-rim artifact in first-pass myocardial perfusion MRI: Removing Gibbs ringing effects using optimized radial imaging. Magn Reson Med. 2013 doi: 10.1002/mrm.24913.
34. Sharif B, Dharmakumar R, LaBounty T, Shufelt C, Thomson L, Merz N, Berman DS, Li D. Projection imaging of myocardial perfusion: minimizing the subendocardial dark-rim artifact. J Cardiovasc Magn Reson. 2012; 14(Suppl 1):P275.
35. Sharif B, Dharmakumar R, LaBounty T, Shufelt C, Thomson LE, Merz NB, Berman DS, Li D. Eliminating dark-rim artifacts in first-pass myocardial perfusion imaging. J Cardiovasc Mag Res. 2013; 15(Suppl 1):O3.
36. Salerno M, Sica C, Kramer CM, Meyer CH. Improved first-pass spiral myocardial perfusion imaging with variable density trajectories. Magn. Reson. Med. 2013 doi: 10.1002/mrm.24569.

37. Fessler JA. On NUFFT-based gridding for non-Cartesian MRI. J Magn Reson. 2007; 188:191–195. [PubMed: 17689121]

38. Fenchel M, Helber U, Simonetti OP, Stauder NI, Kramer U, Nguyen CN, Finn JP, Claussen CD, Miller S. Multislice first-pass myocardial perfusion imaging: Comparison of saturation recovery (SR)-TrueFISP-two-dimensional (2D) and SR-TurboFLASH-2D pulse sequences. J Magn Reson Imaging. 2004; 19:555–563. [PubMed: 15112304]

39. Schabel MC, Parker DL. Uncertainty and bias in contrast concentration measurements using spoiled gradient echo pulse sequences. Phys. Med. Biol. 2008; 53:2345–2373. [PubMed: 18421121]

40. Bassingthwaighte JB, Malone MA, Moffett TC, King RB, Chan IS, Link JM, Krohn KA. Molecular and particulate depositions for regional myocardial flows in sheep. Circ. Res. 1990; 66:1328–1344. [PubMed: 2335030]

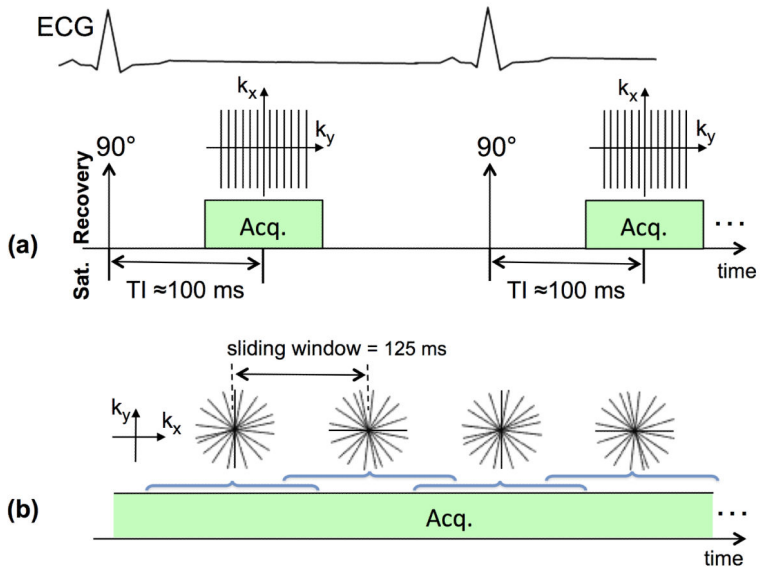

Figure 1.

Description of the “conventional” and the proposed non-ECG-gated “continuously-sampled” first-pass perfusion pulse sequences. **(a)** Conventional pulse sequence: ECG-gated FLASH with saturation recovery (SR) magnetization preparation; typically, an undersampled Cartesian k-space is acquired (reconstructed using parallel imaging), synchronized with the ECG gating signal at a pre-defined TI time (e.g., 100 ms). **(b)** Proposed “continuously-sampled” pulse sequence: non-ECG-gated FLASH (optimized flip angle) with continuous acquisition of a 2D golden-angle radial k-space trajectory (111.246° angular spacing between consecutive projections). A sliding window (125 ms temporal shifts) is applied to reconstruct one frame from consecutive projections without any temporal acceleration, resulting in 8 frames per second. No external ECG signal or other forms of cardiac synchronization is needed for the proposed method.

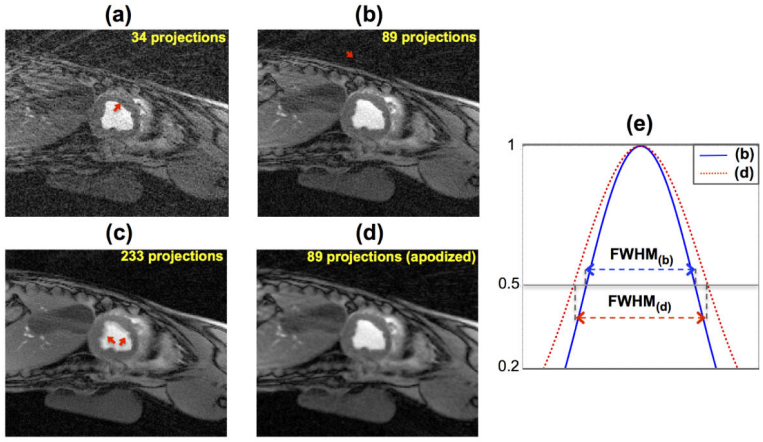

Figure 2.

Demonstration of the methodology for retrospective selection of reconstruction parameters using the properties of golden-angle radial acquisition: all images correspond to a similar time-point in the continuously-sampled FPP scan (10 seconds after start of the scan, prior to the myocardial enhancement phase) in one of the ischemic dog studies (average heart rate: 98 bpm). **(a,b,c):** Standard regridding with 34, 89, and 233 projections, respectively (same gray-scale; in-plane resolution: 1.4 × 1.4 mm^2); the arrows in (a)-(b) point to streaking artifacts in the myocardium and outside of the heart region, and those in (c) point to blurring at the endocardial wall caused by the large temporal window (582 ms). **(d):** Apodized regridding reconstruction using a Gaussian kernel as the apodizing function. The SNR (ratio of mean to standard deviation of signal intensity in the septum) for (a)-(d) are 3.6, 8.7, 15.1, and 14.9, respectively. **(e):** Demonstration of the effect of apodization on the reconstructed resolution; the plot shows 1D cut of the main lobe of the point spread function (PSF) corresponding to the reconstructions in (b) and (d). This plot only shows a fraction of the central region of the PSFs to allow for visualization of the FWHM differences. The ratio of the FWHM for (d) relative to (b) is 1.2, which implies an in-plane resolution of 1.7×1.7 mm^2 for the apodized reconstruction in (d). Comparing (b) and (d), apodization results in improved SNR (reduced streaking) at the cost of spatial resolution (1.2-fold widening of FHWM as shown in (e)); nevertheless, the reconstructed resolution after apodization (1.7×1.7 mm^2) in (d) is significantly higher than conventional FPP methods.

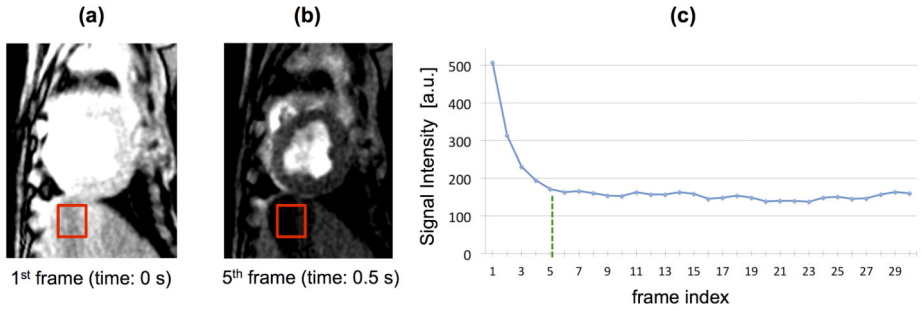

Figure 3.

Verification of fast transition to approximate steady state for the imaged slice. **(a)** and **(b)** show the 1st and 5th reconstructed frames for one of the animal studies with coronary stenosis, corresponding to the 0 s and 0.5 s time points during the continuously-sampled scan, respectively. The windowing is kept the same for the two frames and the highlighted box shows a selected ROI adjacent to the heart. **(c)** Average signal intensity (SI) in the ROI for the first 30 frames (not scaled, arbitrary units). The fast transition to steady state can be seen by comparing (a) and (b) and also by observing the SI behavior in (c). The mean SI in the ROI for the 5th frame shown in (b) is only 15% higher than the estimated steady state value (estimated as the mean ROI intensity averaged over the last 10 frames).

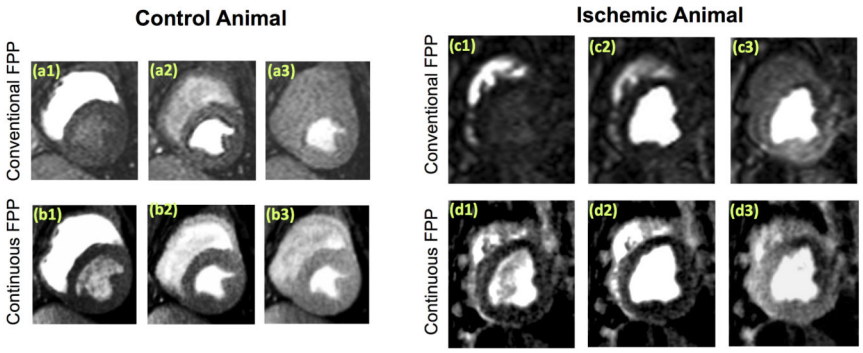

Figure 4.

First-pass perfusion images from the control study and one of the ischemic (LAD stenosis) animal studies. The continuously-sampled frames were selected to closely match the cardiac phase and contrast enhancement phase of the corresponding conventional FPP images. The 1st, 2nd, and 3rd columns show example images from the RV, LV, and myocardial enhancement phases in the FPP series, respectively: **(a1)-(a3):** conventional scan, control dog, heart rate (HR): 58 bpm; **(b1)-(b3):** continuously-sampled scan, control dog, HR: 57 bpm; **(c1)-(c3)** conventional scan, ischemic dog, HR: 95 bpm; **(d1)-(d3)** continuously-sampled scan, ischemic dog, HR: 98 bpm. The in-plane spatial resolution for the continuously-sampled and conventional FPP images are 1.7×1.7 mm^2 and 2.4×1.8 mm^2, respectively. Windowing is the same for each row but varies row to row. The continuously-sampled frames are artifact-free and the perfusion defect area in (c3) closely matches the one in (d3).

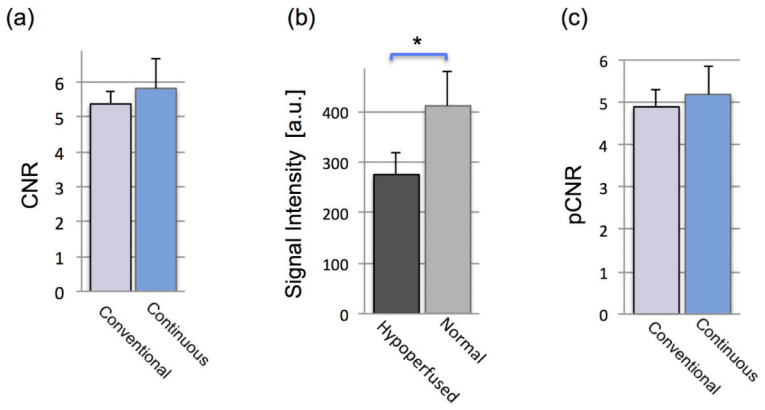

Figure 5.

(a): Comparison of image quality in terms of contrast-to-noise ratio (CNR) across all animal studies (n=5) where CNR is defined as in (37) to be the difference in the myocardial SNR (measured in a septal region-of-interest as in Fig. 2) between the peak enhancement phase the pre-contrast phase (continuous: 5.82±0.92 vs. conventional: 5.36±0.36; p=0.34). **(b,c):** Summary of the image contrast analysis for the ischemic dog studies (n=4) comparing the proposed continuously-sampled FPP method and the conventional method; **(b):** Average myocardial signal intensity in the hypoperfused (ischemic) and normal (remote) regions for the representative continuously-sampled FPP images (normal: 410±69 vs. hypoperfused: 276±42; p<0.005); **(c)**: Hypoperfused-to-normal CNR (pCNR) for the continuously-sampled FPP images versus the conventional FPP images. Overall, the continuously-sampled FPP images have a similar pCNR compared to the conventional FPP images (continuous: 5.18±0.70 vs. conventional: 4.88±0.43; p=0.32).

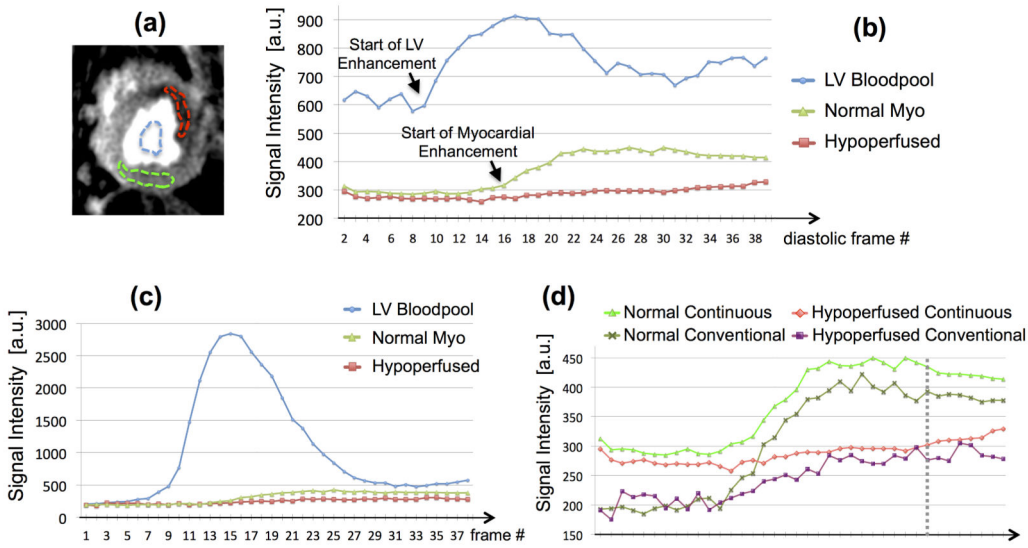

Figure 6.

(a,b) Example SI-time curves for the proposed continuously-sampled FPP method: **(a)** selected ROIs in the LV bloodpool, remote region (normal perfusion), and ischemic region (hypoperfusion) for one of the ischemic animals (same as Fig. 4); **(b)** mean SI in each region (arbitrary units, same scale for all plots) as a function of time for manually-selected diastolic frames (1 frame per cardiac cycle among 8 frames/s; 38 cardiac cycles are shown; average HR: 98 bpm). Arrows in (b) point to start of LV bloodpool and myocardial enhancement. **(c)** SI-time curves for the corresponding conventional scan (average HR: 95 bpm). **(d)** Myocardial SI-time curves from (b) and (c) overlaid with no rescaling. The dotted line in (d) highlights the myocardial enhancement phase (Panels (c3) and (d3) in Fig. 4), and demonstrates the similar SI difference (contrast) between the normal and hypoperfused curves. The myocardial SI-time curves for the continuously-sampled method show a slower contrast uptake for the ischemic region compared to the remote region, which is consistent with the conventional scan. However, the bloodpool SI for the continuously-sampled method exhibits significantly higher saturation effects compared to the conventional method.